iScience

Article

Hyperandrogenism triggers mtDNA release to participate in ovarian inflammation via mPTP/cGAS/STING in PCOS

Graphical abstract

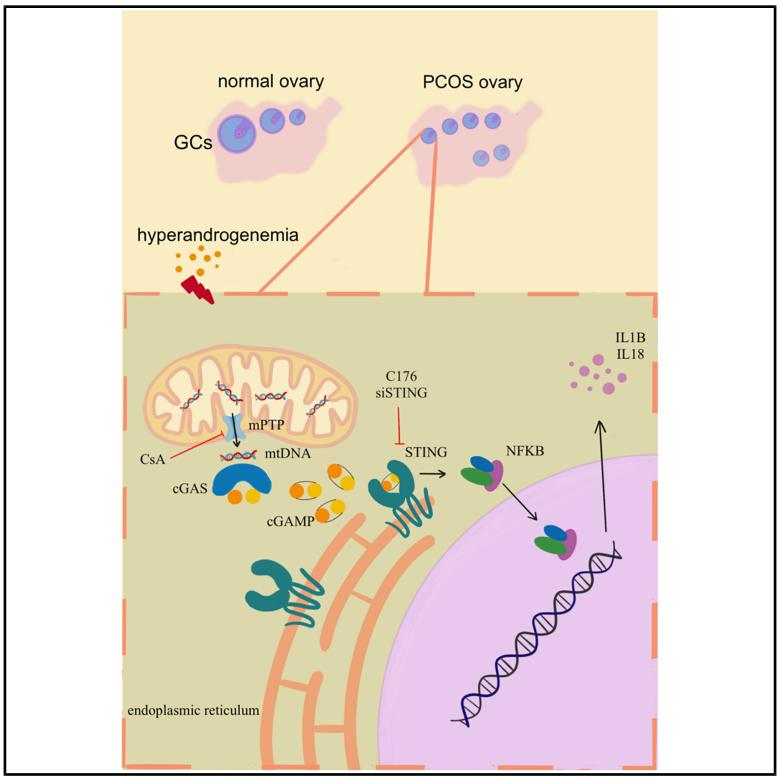

Authors

Jieyu Cai, Qi Zhu, Yu Xiang, ..., Xiaoqi Hong, Mingrui Xue, Hongshan Ge

Correspondence

hongshange@njmu.edu.cn

In brief

Endocrinology; Female reproductive endocrinology; Molecular biology

Highlights

- Excessive accumulation of mtDNA in human ovarian granule cytoplasm
- Cytoplasmic free mtDNA increased after testosterone stimulation of KGN cells
- MtDNA activates inflammation in KGN cells through the cGAS-STING pathway
- Targeting cGAS-STING pathway can improve inflammation and follicle dysfunction in PCOS mice

Cai et al., 2025, iScience *28*, 112391
May 16, 2025
https://doi.org/10.1016/j.isci.2025.112391

CellPress

iScience

CellPress
OPEN ACCESS

Article

Hyperandrogenism triggers mtDNA release to participate in ovarian inflammation via mPTP/cGAS/STING in PCOS

Jieyu Cai,[1,2,5] Qi Zhu,[2,3,5] Yu Xiang,[2,5] Linglin Weng,[1,2] Na Liang,[2,4] Xiaoqi Hong,[2,3] Mingrui Xue,[2,4] and Hongshan Ge[1,2,3,4,6,*]

[1]Graduate School, Nanjing University of Chinese Medicine, Nanjing, China
[2]Reproduction Medicine Centre, Nanjing Medical University Affiliated Taizhou People's Hospital, Taizhou, China
[3]Graduate School, Nanjing Medical University, Nanjing, China
[4]Graduate School, Dalian Medical University, Dalian, China
[5]These authors contributed equally
[6]Lead contact
*Correspondence: hongshange@njmu.edu.cn
https://doi.org/10.1016/j.isci.2025.112391

SUMMARY

Hyperandrogenism induced ovarian inflammation is associated with the pathogenesis of polycystic ovary syndrome (PCOS), but the specific mechanism behind it remains unclear. The aim of this study was to elucidate the association between mitochondrial DNA-cGAS-STING pathway and PCOS inflammatory response. RNA sequencing analysis and other experiments showed that inflammatory pathways were activated, mitochondria were damaged, and mtDNA-cGAS-STING pathways were activated in PCOS women. *In vitro*, after stimulation of KGN cells with testosterone, the expression of pro-inflammatory factors was enhanced and the cGAS-STING pathway was activated. Stimulator of the interferon genes (STING) knockout can reduce testosterone-induced inflammatory response and improve follicular function. Cyclosporin A therapy reduces cytoplasmic mtDNA, blocks cGAS-STING pathway activation, alleviates inflammatory markers, and reverses abnormal follicular function. *In vivo* experiments have shown that inhibiting STING can reduce ovarian dysfunction and inflammation in PCOS patients. Hyperandrogenism in PCOS can trigger mitochondrial permeability transition pore (mPTP) overopening, leading to mtDNA release and cGAS-STING pathway activation, causing inflammation and follicle damage.

INTRODUCTION

Polycystic ovary syndrome (PCOS), a prevalent endocrine disorder affecting women of reproductive age, is characterized by hyperandrogenism, ovulatory dysfunction, and polycystic ovaries.[1,2] PCOS is a major issue within gynecological endocrinology, precipitating a spectrum of reproductive dysfunctions, including oligomenorrhea, amenorrhea, and anovulatory infertility.[2–4] This multifaceted disorder exerts its influence across a broad population, with epidemiological data indicating that it affects a significant proportion of women—with global prevalence ranging from 4% to 21%.[5] PCOS is a complex syndrome with a heterogeneous presentation, making it challenging to delineate a single underlying pathophysiological mechanism. Current theories suggest that PCOS arises from a combination of genetic predispositions, environmental factors, and metabolic disturbances. Central to the PCOS pathogenesis is an imbalance in the hypothalamic-pituitary-ovarian axis, leading to hyperandrogenism and anovulation.[6] This hormonal imbalance is often accompanied by insulin resistance and compensatory hyperinsulinemia, which further exacerbate androgen production.[7]

Follicular dysplasia is a pivotal factor contributing to anovulation and infertility among women with PCOS. The ovaries of patients with PCOS show abnormal activation of numerous antral follicles, which remain at the 2–8 mm stage, indicating a failure in dominant follicle selection and arrested growth of larger follicles (5–8 mm), culminating in polycystic ovarian morphology. This aberrant development disrupts the normal follicular recruitment, selection, and dominance processes.[8,9] The molecular and cellular mechanisms underlying follicular dysregulation in PCOS are incompletely understood, hindering clinical treatment progress for PCOS-associated infertility.

The follicular microenvironment, particularly its inflammatory milieu, is critical for follicle development, maturation, and ovulation. Optimal inflammation is necessary for these processes, whereas sustained inflammation can adversely affect the follicular environment and impede follicular development and ovulation.[10,11] Our research has demonstrated that hyperandrogenemia induces ovarian inflammation and triggers granulosa cells (GCs) pyroptosis, which may contribute to the etiology of follicular dysplasia in PCOS.[12] Thus, the specific molecular

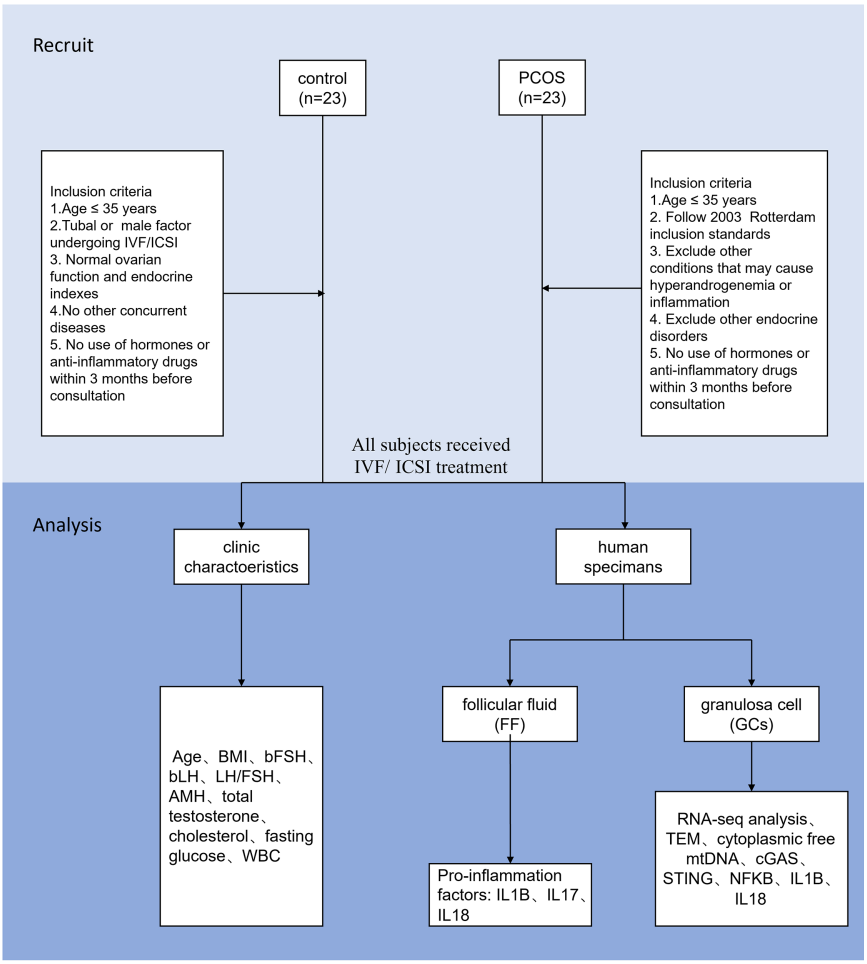

Figure 1. The flow chart about the research of clinical samples

The chart details the criteria for inclusion and exclusion of clinical samples and the experiments performed after obtaining the samples.

mechanisms through which hyperandrogenemia initiates inflammation in the ovarian microenvironment warrant further elucidation.

Mitochondria are involved in energy production, as well as cellular signaling and innate immunity.[13,14] Mitochondrial DNA (mtDNA), a circular genome encoding 13 proteins, 22 tRNAs, and 2 rRNAs, is particularly vulnerable to oxidative stress due to its proximity to the electron transport chain.[15] Under conditions of cellular stress, damage, or apoptosis, mtDNA can be released into the cytosol, where it can activate the cyclic GMP-AMP synthase (cGAS), a stimulator of the interferon genes (STING) pathway.[16] This pathway has recently emerged as a critical mediator of innate immune responses, particularly in the context of cytosolic DNA sensing.[17] Several mechanisms have been proposed for the release of mtDNA into the cytosol, including the formation of membrane pores, mitochondrial fission, and activation of the mitochondrial permeability transition pore (mPTP).[16] Once in the cytosol, mtDNA can act as a potent activator of cGAS. Upon binding to cytosolic DNA, cGAS catalyzes the synthesis of cyclic GMP-AMP (cGAMP), which subsequently binds to and activates STING.[18] This activation induces a conformational change in STING, leading to its translocation from the endoplasmic reticulum (ER) to the Golgi apparatus. At the Golgi, STING recruits and activates the TANK-binding kinase 1 (TBK1), which in turn phosphorylates interferon regulatory factor 3 (IRF3) and nuclear factor-kappa B (NFKB). Phosphorylated NFKB (pNFKB) dimerizes and translocates to the nucleus, where it induces the transcription of type I interferons and other pro-inflammatory cytokines.[19,20]

Mitochondrial dysfunction has been implicated in the pathogenesis of various metabolic and inflammatory diseases, including PCOS.[21] Altered mitochondrial function and morphology have been shown in ovarian tissue of women with PCOS, including increased mitochondrial biogenesis and oxidative stress.[22] These changes may lead to mtDNA release into the cytosol, where it can activate the cGAS-STING pathway and contribute to the inflammatory state observed in PCOS. However, the molecular mechanisms underlying the initiation and perpetuation of this inflammatory state in PCOS are not well described. Herein, we tested the hypothesis that cytosolic escape of mtDNA is a trigger for cGAS-STING-dependent inflammation in PCOS.

RESULTS

Inflammation pathway activation in follicles of patients with PCOS

We first collected GCs from women diagnosed with PCOS and age-matched healthy controls, all of whom were undergoing *in vitro* fertilization (IVF)/intracytoplasmic sperm injection (ICSI) treatment (Figure 1), for RNA-seq analysis. Comparative genomic and functional annotation analyses, utilizing Gene Ontology (GO) and Kyoto Encyclopedia of Genes and Genomes (KEGG). GO results showed that PCOS was revealed a significant activation of inflammatory (Figure 2A), while KEGG results also showed that PCOS was associated with inflammatory pathways, such as NFKB pathway (Figure 2B). Meanwhile, the clinical data we collected also showed that the level of white blood cells in the PCOS group was significantly increased, indicating that PCOS patients were in a state of inflammation (Table 1).

Next, we collected follicular fluid (FF) and quantified the levels of pro-inflammatory biomarkers IL1B, IL17, and IL18. Elevated levels of these biomarkers in the FF of PCOS further

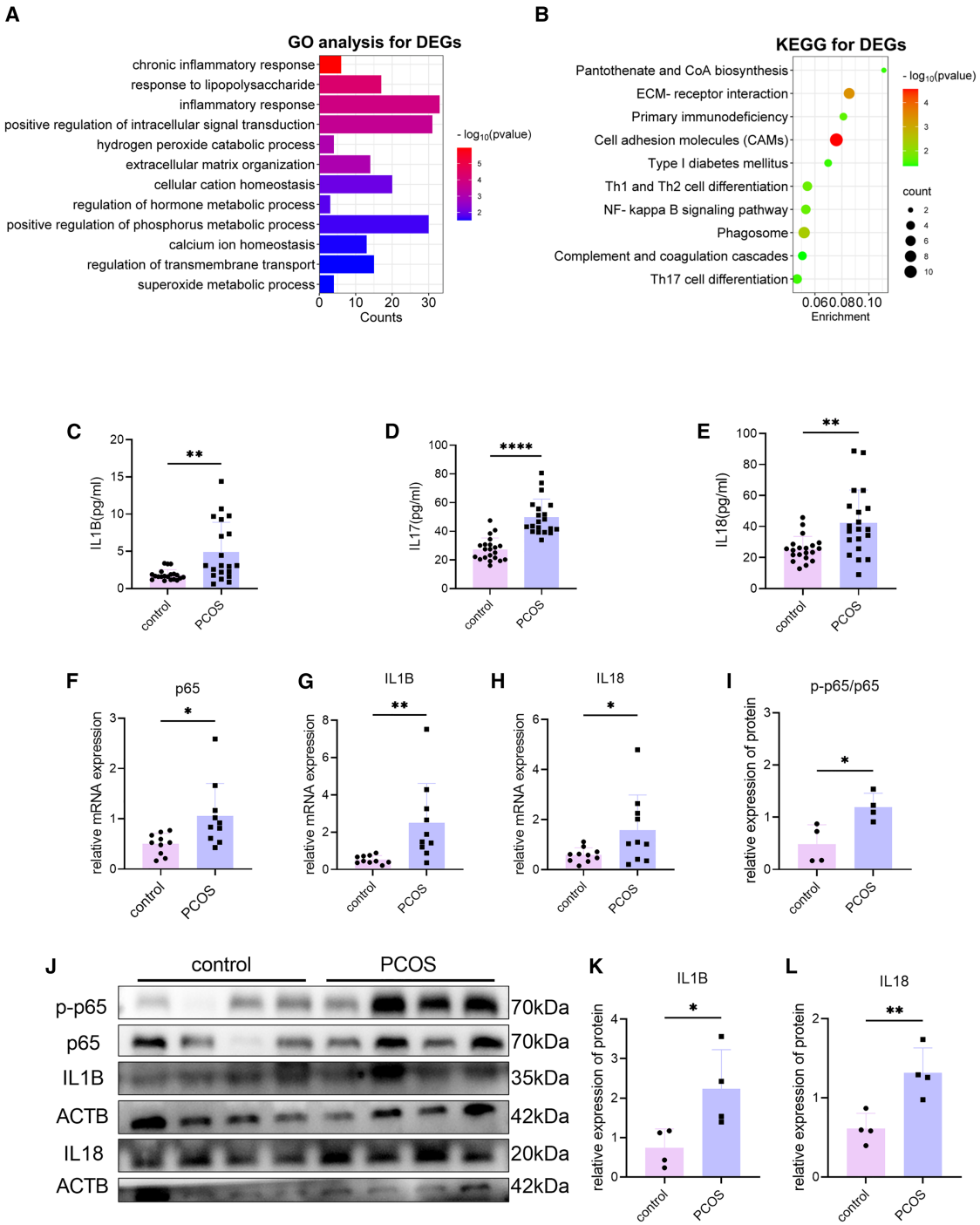

Figure 2. Activation of inflammation in FF and GCs cells in patients with PCOS

(A) Functional annotation for GCs-related genes using GO enrichment analysis (n = 3).

(B) Enriched pathways in KEGG analysis of GCs (n = 3).

(C) Levels of IL1B in FF (n = 20).

(D) Levels of IL17 in FF (n = 20).

(E) Levels of IL18 in FF (n = 20).

(F) mRNA levels of p65 in GCs in patients with PCOS and controls (n = 10).

(G) mRNA levels of IL1B in GCs in patients with PCOS and controls (n = 10).

(H) mRNA levels of IL18 in GCs in patients with PCOS and controls (n = 10).

(I) Quantification of protein expression levels of p-p65/p65 in GCs of patients with PCOS compared with controls (n = 4).

(legend continued on next page)

Table 1. The clinical characteristics of PCOS patients and control

Parameters	Control (n = 23)	PCOS (n = 23)	p value
Age (years)	29.61 ± 2.90	29.04 ± 3.18	0.533
BMI (kg/m^2)	21.53 ± 2.83	24.44 ± 4.20	0.018*
FSH (IU/L)	7.69 ± 2.70	6.00 ± 1.62	0.014*
LH (IU/L)	4.18 ± 1.67	8.10 ± 1.53	<0.001***
LH/FSH	0.64 ± 0.40	1.50 ± 1.01	<0.001***
AMH (ng/mL)	3.78 ± 0.84	6.27 ± 1.02	<0.001***
Total testosterone (ng/mL)	1.37 ± 0.45	2.43 ± 0.17	<0.001***
Estradiol (pmol/L)	210.9 ± 80.27	172.3 ± 65.89	0.093
Progesterone (nmol/L)	1.99 ± 1.00	1.67 ± 0.95	0.281
Cholesterol (mmol/L)	4.58 ± 0.88	5.29 ± 1.06	0.017*
Fasting glucose (mmol/L)	5.15 ± 0.39	5.60 ± 0.69	0.009**
WBC (10^9/L)	5.03 ± 1.36	6.80 ± 1.93	<0.001***

corroborated the presence of a pro-inflammatory response (Figures 2C–2E).

Phosphorylation and translocation of p65 to the nucleus is the most typical manifestation of NFKB pathway activation, so this study focused on p65. Finally, we evaluated the expression levels of p65, IL1B, and IL18 in both mRNA and protein forms within the GCs. Comparative analysis demonstrated significantly higher levels of p65, IL1B, and IL18 in the GCs of patients with PCOS compared with healthy controls (Figures 2F–1L). These findings reinforce the notion that inflammation is a characteristic feature within the follicular environment of patients with PCOS.

Mitochondrial damage, mtDNA release, and cGAS-STING activation in GCs of patients with PCOS

Multiple studies have shown that mitochondria play a vital role in inflammation, with the release of mtDNA from damaged mitochondria serving as a key inflammatory mediator.[16] Additionally, our previous research has demonstrated that damage to ovarian mitochondrial structure and function is associated with PCOS.[23] Herein, we further compared the structural integrity of mitochondria in the GCs of patients with PCOS and healthy control women using electron microscopy. The results revealed that mitochondria in GCs of healthy controls exhibited normal morphology, characterized by rounded or oval shapes with well-organized cristae (Figure 3A, upper panel). Conversely, mitochondria in the GCs of patients with PCOS displayed signs of disarray, including swelling, irregular morphology, discontinuous, and ruptured membranes (Figure 3A, lower panel). These findings suggest significant mitochondrial injury to the mitochondrial membranes in GCs of patients with PCOS, which may lead to the release of mitochondrial contents.

Next, to investigate whether damage to the mitochondrial ultrastructure could result in an augmented release of mtDNA from mitochondria, we further quantified cytoplasmic mtDNA levels in the GCs of patients with PCOS. DNA was extracted from the cytoplasm and analyzed using qPCR. The nuclear gene B2M served as an internal control, while mtDNA was specifically amplified using ND1 and D loop primers. The analysis revealed significantly higher levels of cytoplasmic-free mtDNA in the GCs of patients with PCOS, suggesting a potential correlation between incomplete mitochondrial structural integrity and increased mtDNA release in the GCs of women with PCOS (Figures 3B and 3C).

Previous research has indicated that cytosolic mtDNA is sensed by receptors, such as cGAS, activating STING, and initiating inflammatory signaling. Thus, we further compared the expressions of cGAS and STING in the GCs of patients with PCOS and healthy controls. Our analysis revealed markedly increased protein expression levels of both cGAS and STING in the former group (Figures 3D and 3E). Collectively, these findings suggest that the cGAS-STING pathway is activated in the GCs of patients with PCOS, potentially contributing to the pathophysiology of the syndrome.

T-induced mtDNA releasing triggered inflammation via cGAS-STING pathway in KGN cells

To investigate the correlation between mtDNA release, activation of the cGAS-STING signaling pathway, and inflammation, we established an *in vitro* model utilizing T. Specifically, we exposed KGN cell, a line of human GCs, to a high concentration of T (10 μM) to mimic the elevated androgen levels observed in women with PCOS. Following 24 h of incubation with T, we observed a significant increase in the mRNA and protein levels of inflammatory markers p65, IL1B, and IL18 compared with the control group (Figures 4A–4C). These results suggest that a high-androgen environment may promote ovarian cell inflammation. Additionally, T treatment led to increased cytoplasmic mtDNA and activation of proteins involved in the cGAS-STING pathway, as evidenced by GCs from patients with PCOS

(J) Representative WB images of p-p65, p65, IL1B, and IL18 in GCs in patients with PCOS and controls.
(K) Quantification of protein expression levels of IL1B in GCs of patients with PCOS compared with controls (n = 4).
(L) Quantification of protein expression levels of IL18 in GCs of patients with PCOS compared with controls (n = 4).
Data are represented as mean ± SEM.*p < 0.05, **p < 0.01, ***p < 0.001, ****p < 0.0001.

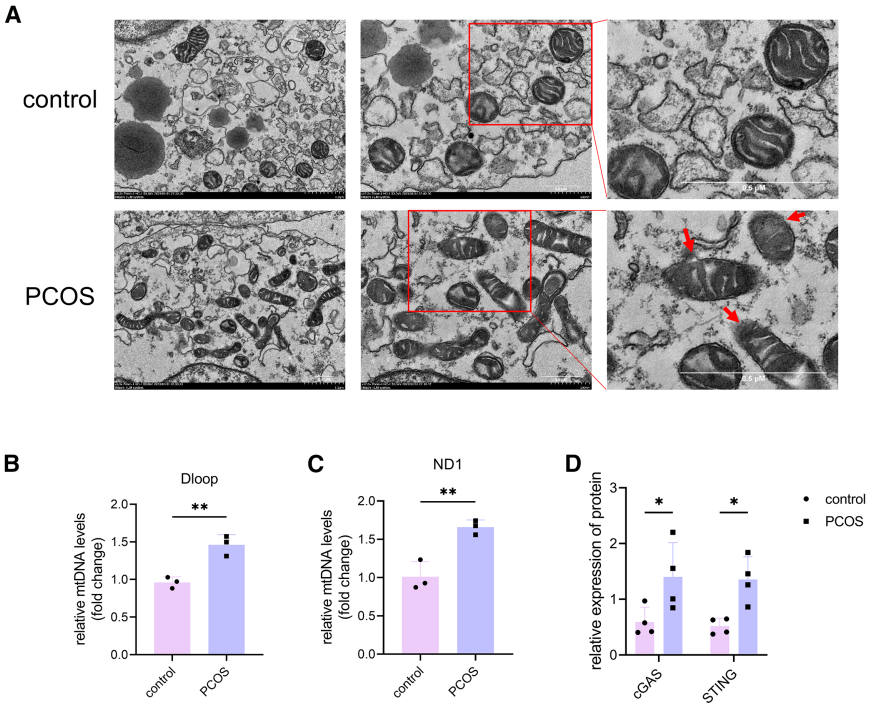

Figure 3. Mitochondrial damage, release of mtDNA, and activation of cGAS-STING pathway in GCs of patients with PCOS

(A) Representative transmission electron microscopy images of mitochondria in GCs of patients with PCOS and controls (scale bar, 0.5 μm).

(B) RT-qPCR quantitative analysis of cytosolic mtDNA (D Loop) normalized to nuclear gene (B2M) of total lysates from GCs of patients with PCOS and controls ($n = 3$).

(C) RT-qPCR quantitative analysis of cytosolic mtDNA (ND1) normalized to nuclear gene (B2M) of total lysates from the GCs in patients with PCOS and controls ($n = 3$).

(D) Quantification of protein expression levels of cGAS and STING in GCs of patients with PCOS compared with controls ($n = 3$).

(E) Representative WB images of cGAS and STING in GCs of patients with PCOS and controls. Data are represented as mean ± SEM.*$p < 0.05$, **$p < 0.01$.

(Figures 4D–4G). Immunofluorescence revealed that cGAS expression was upregulated in KGN cells after T stimulation (Figure 4H and 4I).

Previous studies have demonstrated that mtDNA release from hepatocytes contributes to cGAS-STING activation in macrophages.[24] As such, we investigated whether enhanced cGAS-STING activation in GCs was due to increased mtDNA release. To test this hypothesis, mtDNA was isolated and purified from kidney epithelial cells, then transfected into KGN cells. Western Blot (WB) analysis was subsequently used to assess the expressions of cGAS, STING, and inflammatory markers. The results showed that following mtDNA stimulation, expressions of cGAS and STING increased, as did the levels of p-p65, IL1B, and IL18 (Figures 4J–4L).

These cumulative findings indicate that high androgen levels may trigger ovarian inflammation by promoting mtDNA escape, which subsequently activates the cGAS-STING pathway and further inflammation.

Inhibiting STING alleviated T-induced inflammation and dysfunction of KGN cells

The cGAS-STING pathway is a critical component of the innate immune response that is activated by the detection of cytoplasmic DNA, resulting in the initiation of an inflammatory cascade. However, it has remained unclear whether this pathway also exerts similar inflammatory activation effects in ovarian GCs. To investigate this, we silenced STING expression in KGN cells using siRNA, leading to a significant decrease in p65, IL1B, and IL18; this suggests that the cGAS-STING pathway has a role in activating these pro-inflammatory markers (Figures 5A–5C). Additionally, we examined p65 translocation and found that T stimulation prompted its movement from the cytoplasm to the nucleus. However, this effect was significantly reduced upon STING knockdown, indicating the cGAS-STING pathway may be crucial for the full activation of NFKB by T stimulation (Figures 5D and 5E).

However, whether the inflammation induced in GCs by cGAS-STING pathway activation affects follicular function remained unclear. Therefore, we further analyzed the effect of STING knockdown on ovarian function by examining key genes related to follicular formation and steroidogenesis, including NR3C4 (AR), follicle-stimulating hormone receptor (FSHR), HSD3B2, and CYP11A1. Our results showed a significant increase in these genes after T stimulation, which were significantly reduced upon STING silencing. This suggests that the cGAS-STING pathway modulates the expression of genes essential for normal follicle development and steroidogenesis (Figures 5F–5I).

In conclusion, these findings highlight the dual role of the cGAS-STING pathway in regulating both inflammation and follicle function, which could significantly contribute to the understanding and management of PCOS.

Pharmacologically blocking KGN cell mPTP ameliorated T-induced mtDNA release, cGAS-STING activation, inflammation, and dysfunction

mtDNA is usually enclosed by the inner mitochondrial membrane (IMM), effectively preventing its escape.[25] However, mtDNA escape into the cytoplasm needs to go through mPTP, which is located within the IMM. Previous research has suggested

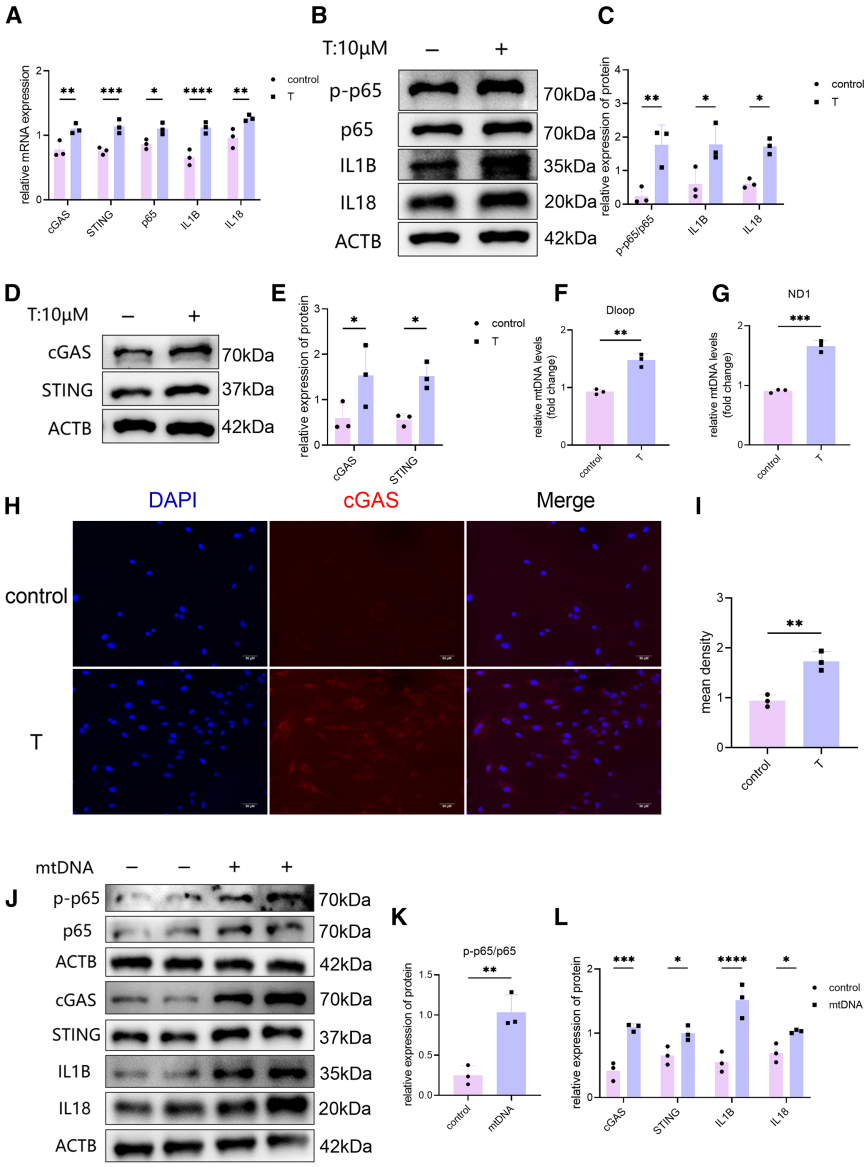

Figure 4. mtDNA release-induced activation of inflammation and cGAS-STING pathway in T-induced KGN cells *in vitro*

(A) mRNA levels of cGAS, STING, p65, IL1B, and IL18 in KGN cells exposed to T compared with controls ($n = 3$).

(B) Representative western blotting images of p-p65, p65, IL1B, and IL18 in GCs of KGN cells exposed to T compared with controls.

(C) Quantification of protein expression levels of p-p65/p65, IL1B, and IL18 in KGN cells exposed to T compared with controls ($n = 3$).

(D) Representative western blotting images of cGAS and STING in GCs in KGN cells exposed to T compared with controls.

(E) Quantification of protein expression levels of cGAS and STNG in KGN cells exposed to T compared with controls ($n = 3$). (F) RT-qPCR quantitative analysis of cytosolic mtDNA (D Loop) normalized to nuclear gene (B2M) of total lysates from the KGN cells exposed to T compared with controls ($n = 3$).

(G) RT-qPCR quantitative analysis of cytosolic mtDNA (ND1) normalized to nuclear gene (B2M) of total lysates from the KGN cells exposed to T compared with controls($n = 3$).

(H) Representative fluorescence images of cGAS in KGN cells exposed to T compared with controls (scale bar, 50 μm).

(I) Quantitative analysis of fluorescence intensity for cGAS in KGN cells exposed to T compared with controls ($n = 3$).

(J) Representative western blotting images of cGAS, STING, p-p65, p65, IL1B, and IL18 after mtDNA transfection of KGN cells ($n = 3$, mtDNA 1 μg/mL for 24 h).

(K) Quantification of protein expression levels of p-p65/p65 after mtDNA transfection of KGN cells ($n = 3$).

(L) Quantification of protein expression levels of cGAS, STING, IL1B, and IL18 after mtDNA transfection of KGN cells ($n = 3$). T, testosterone; Data are represented as mean ± SEM.*$p < 0.05$, **$p < 0.01$, ***$p < 0.001$, ****$p < 0.0001$.

that abnormal mPTP opening is linked to mtDNA leakage.[26] Nevertheless, it has been unclear whether the abnormal release of mtDNA from the GCs of patients with PCOS is associated with mPTP dysfunction.

To investigate this, we initially employed an mPTP assay kit to quantify the degree of mPTP opening in KGN cells. The findings demonstrated a significant augmentation in mPTP opening in KGN cells after T treatment (Figures 6A and 6B). Next, to further analyze the relations between mPTP opening and mtDNA release from GCs, and the link between cGAS-STING and inflammation, we employed cyclosporine A (CsA), an mPTP inhibitor, to suppress mPTP opening (Figures 6A and 6B). As expected, CsA treatment led to a significant decrease in cytoplasmic-free mtDNA levels (Figures 6C and 6D). Additionally, downregulation of cGAS, STING, and pro-inflammatory markers was observed following mPTP inhibition (Figures 6E–6H and 7A–7D). Finally, to assess the impact of mPTP opening on ovarian follicle function, we evaluated the expression of key genes involved in follicle development and steroidogenesis after mPTP inhibition. As anticipated, T stimulation significantly increased mRNA levels of NR3C4 (AR), FSHR, HSD3B2, and CYP11A1 in KGN cells, while these genes were downregulated with mPTP inhibition with CsA (Figures 6I–6L).

Consequently, we hypothesized that in PCOS, mitochondrial damage and mPTP opening facilitate the escape of mtDNA into the cytoplasm, activating the cGAS-STING pathway and triggering inflammation, which in turn aggravates follicle dysfunction.

Inhibiting STING alleviated DHEA-induced ovarian dysfunction and inflammation in a PCOS mouse model

In the aforementioned experiment, we demonstrated that the cGAS-STING pathway plays a pivotal role in the inflammatory

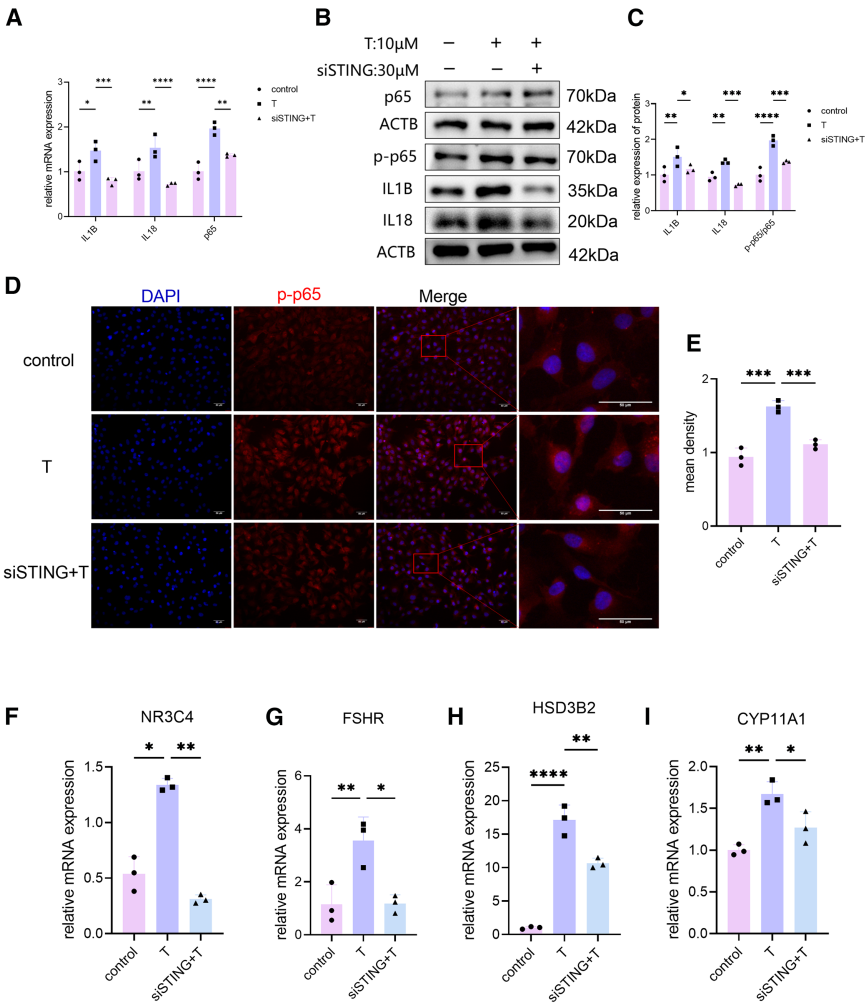

Figure 5. Remission of inflammation and follicle dysfunction following STING inhibition

(A) mRNA levels of p65, IL1B, and IL18 in KGN cells exposed to T after STING knockdown by siRNA (n = 3).

(B) Representative western blotting images of p-p65, p65, IL1B, and IL18 in KGN cells exposed to T after STING knockdown by siRNA.

(C) Quantification of protein expression levels of p-p65/p65, IL1B, and IL18 in KGN cells exposed to T after STING knockdown by siRNA (n = 3).

(D) Representative fluorescence images of p-p65 in KGN cells exposed to T after STING knockdown by siRNA (scale bar, 50 μm).

(E) Quantitative analysis of fluorescence intensity for p-p65 in KGN cells exposed to T after STING knockdown by siRNA (n = 3).

(F) mRNA levels of NR3C4 in KGN cells exposed to T after STING knockdown by siRNA (n = 3).

(G) mRNA levels of FSHR in KGN cells exposed to T after STING knockdown by siRNA (n = 3).

(H) mRNA levels of HSD3B2 in KGN cells exposed to T after STING knockdown by siRNA (n = 3).

(I) mRNA levels of CYP11A1 in KGN cells exposed to T after STING knockdown by siRNA (n = 3). T: testosterone; Data are represented as mean ± SEM.*p < 0.05, **p < 0.01, ***p < 0.001, ****p < 0.0001.

activation triggered by elevated levels of free mtDNA in an *in vitro* model of T-induced PCOS-like GCs. To further substantiate the association between the cGAS-STING pathway and ovarian inflammation, as well as ovarian function in PCOS, we subsequently established an *in vivo* mouse model of PCOS and modulated it using the STING inhibitor C176. The morphological changes of ovary, follicles, and corpus luteum in control group, PCOS group and STING inhibition group were compared. In the control group, different stages of follicle development and an organized granular cell layer were observed. In the PCOS group, cystic follicles were observed in ovaries, the number of GCs in follicles decreased, the number of corpus luteum decreased, oocytes disappeared, and immature small follicles and oblated follicles increased significantly. The previous results were reversed after STING inhibition. By comparing the weight gain of mouse, we found that the weight gain of mouse in PCOS group was significantly higher than that in control group. These indicate that the mouse model was successfully constructed (Figures 8A–8I).

qPCR analysis of PCOS mouse model ovaries revealed that, at the transcriptomic level, inflammatory markers p65, IL1B, and IL18 were significantly upregulated (Figure 8J). Additionally, genes associated with the cGAS-STING signaling pathway exhibited an upregulated expression pattern (Figure 8J). Administration of C176, a specific STING inhibitor, effectively mitigated the elevated levels of these inflammatory markers. WB analysis further corroborated that C176 treatment abrogated the inflammatory activation induced by DHEA (Figures 8K and 8L).

Next, we further analyzed the effects of STING inhibition on ovarian function in mouse by detecting NR3C4, FSHR, HSD3B2, and CYP11A1. Our results showed that these genes were significantly increased after injection of DHEA *in vivo*, but these increases were significantly reduced after inhibition of STING (Figures 8M–8P).

Collectively, these experimental findings underscore the pivotal role of the cGAS-STING pathway in the etiology and progression of PCOS, as well as in the generation of associated inflammatory responses.

DISCUSSION

This study delved into the intricate mechanisms underlying the inflammation observed in PCOS, focusing on the roles of the cGAS-STING pathway and mtDNA.

Follicular dysplasia is a significant contributor to anovulation and infertility in women with PCOS. Despite their importance, the molecular and cellular mechanisms of follicular dysregulation in PCOS have remained elusive. Inflammation, a key player in

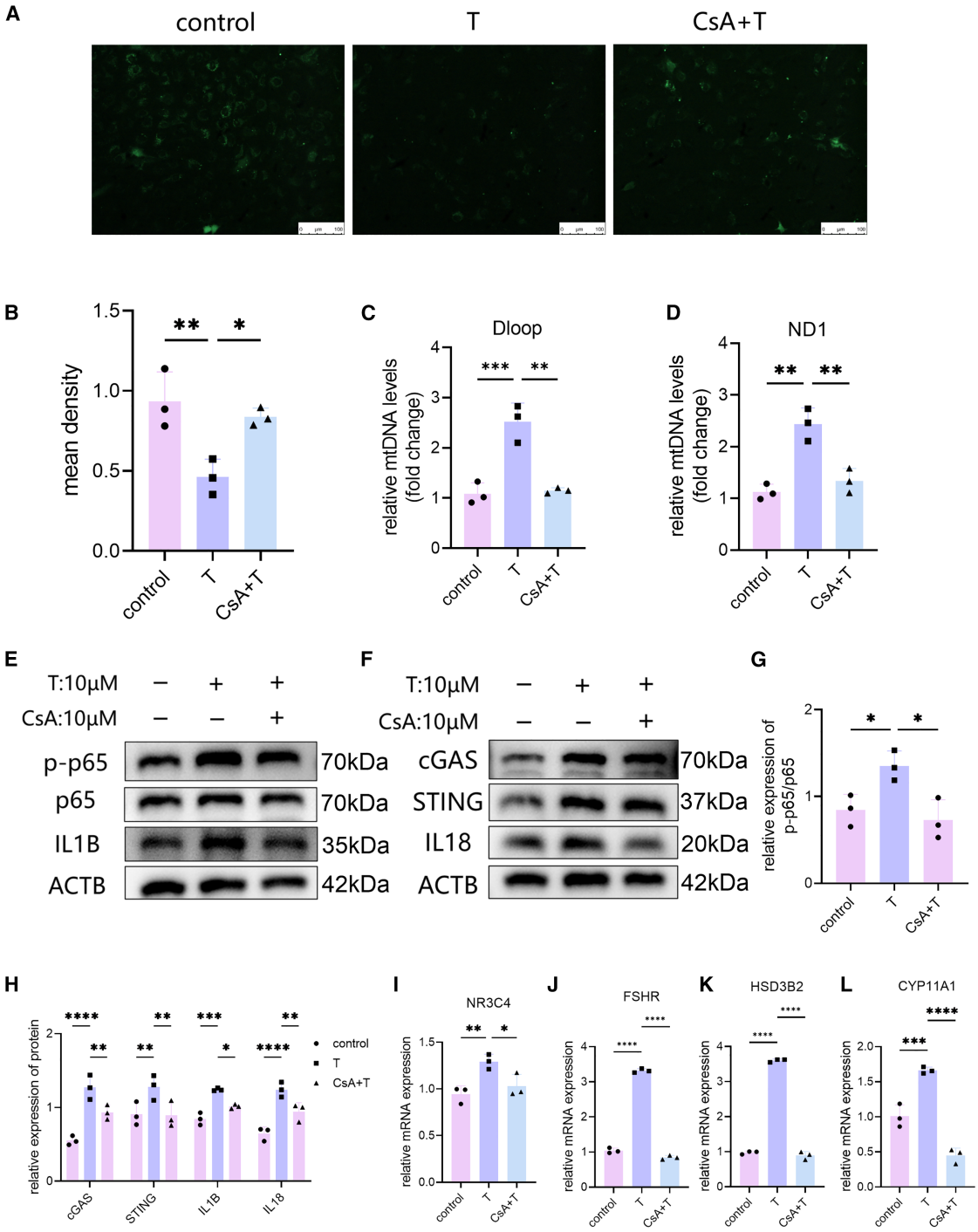

Figure 6. Remission of inflammation and follicle dysfunction following inhibition of opening levels of mPTP

(A) Representative fluorescence images of mPTP opening levels in KGN cells exposed to T and CsA (scale bar, 100 μm).

(B) Quantitative analysis of fluorescence intensity for mPTP opening levels in KGN cells exposed to T and CsA (n = 3).

(C) RT-qPCR quantitative analysis of cytosolic mtDNA (D Loop) normalized to nuclear gene (B2M) of total lysates from the KGN cells exposed to T and CsA (n = 3).

(D) RT-qPCR analysis of cytosolic mtDNA (ND1) normalized to nuclear gene (B2M) of total lysates from the KGN cells exposed to T and CsA (n = 3).

(E) Representative western blotting images of p-p65, p65, and IL1B in KGN cells exposed to T and CsA.

(F) Representative western blotting images of cGAS, STING, and IL18 in KGN cells exposed to T and CsA.

(G) Quantification of protein expression levels of p-p65/p65 in KGN cells exposed to T and CsA (n = 3).

(legend continued on next page)

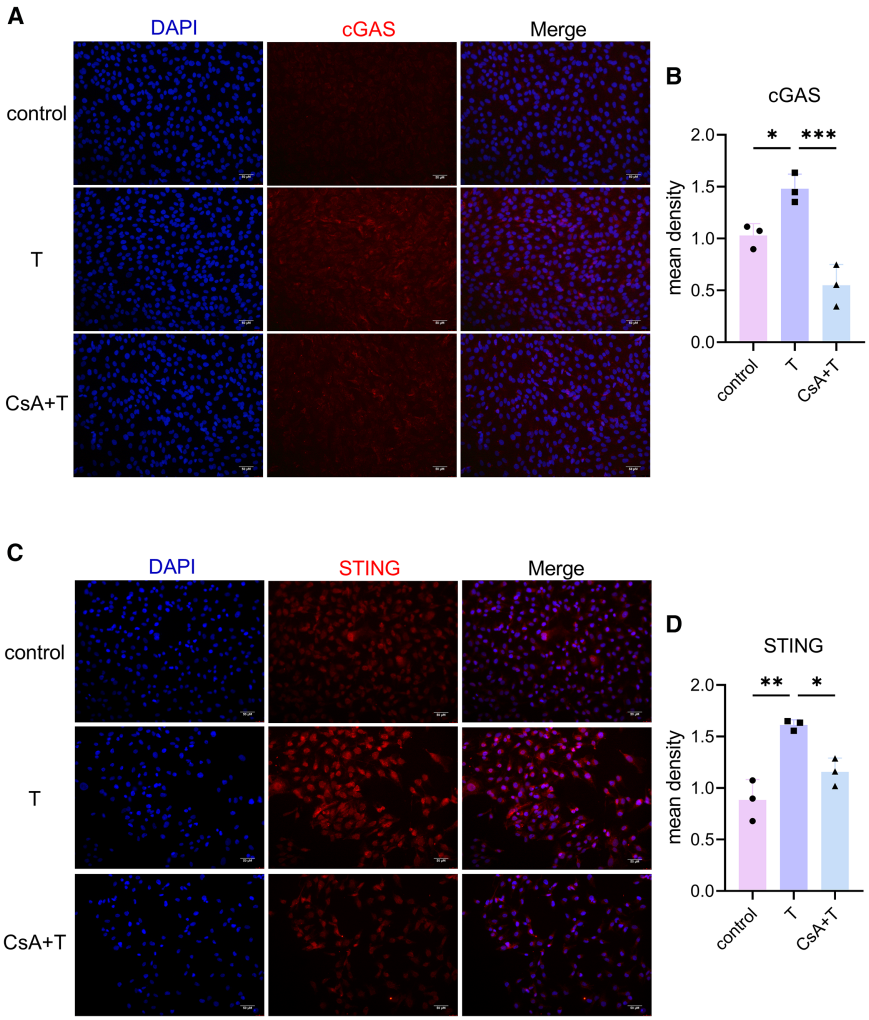

Figure 7. Inhibition of cGAS-STING pathway after reducing of the opening levels of mPTP

(A) Representative fluorescence images of cGAS in KGN cells exposed to T and CsA (scale bar, 50 μm).

(B) Quantitative analysis of fluorescence intensity for cGAS in KGN cells exposed to T and CsA ($n = 3$).

(C) Representative fluorescence images of STING in KGN cells exposed to T and CsA (scale bar, 50 μm).

(D) Quantitative analysis of fluorescence intensity for STING in KGN cells exposed to T and CsA ($n = 3$). T: Testosterone, CsA: Cyclosporin A; Data are represented as mean ± SEM.*$p < 0.05$, **$p < 0.01$, ***$p < 0.001$.

normal ovarian folliculogenesis, can disrupt follicular dynamics when it becomes aberrant.[27] Herein, we applied RNA-seq to discern differential gene expressions in GCs between patients with PCOS and healthy controls. KEGG and GO pathway analysis identified significant upregulation of inflammatory pathways in the GCs of women with PCOS, indicative of a pro-inflammatory state. Subsequent analysis of pro-inflammatory mediators in FF and GCs substantiated these findings, highlighting the pivotal role of inflammation in PCOS-related follicular dysregulation.

Expanding on previous findings of heightened inflammatory markers in PCOS, our study pinpointed an increase in specific cytokines—IL1B, IL17, and IL18—within a sample of patients with PCOS. Their overexpression in PCOS implicates these cytokines in the syndrome's pathogenesis. Furthermore, an increase in p-p65, IL1B, and IL18 in the GCs of patients with PCOS was observed, underscoring the occurrence of a robust intra-follicular inflammatory response. While ovulation is known to induce inflammation, accurately quantifying this in the follicular environment of patients with PCOS is challenging. Nevertheless, our data suggest heightened pro-inflammatory factor expression during the preovulatory phase of PCOS.

Previous studies have established elevated androgen levels as initiators of local follicular inflammation. *In vitro* and *in vivo* models with increased androgen exposure exhibit heightened pro-inflammatory factors in GCs and follicles. Our prior research showed that androgen exposure leads to NFKB, NLRP3, caspase1, and IL1B upregulation in KGN cells, causing GCs pyroptosis and follicular dysfunction. This has also been confirmed in a DHEA-induced PCOS mouse model.[12] The mechanisms linking hyperandrogenism to follicular inflammation activation, however, remain to be elucidated.

Inflammation, frequently arising from the activation of pattern recognition receptors expressed by both immune and non-immune cells, is a complex biological response that can be triggered by PAMPs or DAMPs. Within this intricate regulatory network, mitochondria emerge as pivotal players, transcending their traditional roles in energy metabolism and apoptosis to serve as critical hubs in the modulation of inflammatory processes.[16]

mtDNA, a quintessential DAMP, assumes a paramount position in the orchestration of inflammatory cascades.[28]

(H) Quantification of protein expression levels of cGAS, STING, IL1B and IL18 in KGN cells exposed to T and CsA ($n = 3$). (I) mRNA levels of NR3C4 in KGN cells exposed to T and CsA ($n = 3$).

(J) mRNA levels of FSHR in KGN cells exposed to T and CsA ($n = 3$).

(K) mRNA levels of HSD3B2 in KGN cells exposed to T and CsA ($n = 3$).

(L) mRNA levels of CYP11A1 in KGN cells exposed to T and CsA ($n = 3$). T: Testosterone, CsA: Cyclosporin A; Data are represented as mean ± SEM.*$p < 0.05$, **$p < 0.01$, ***$p < 0.001$, ****$p < 0.0001$.

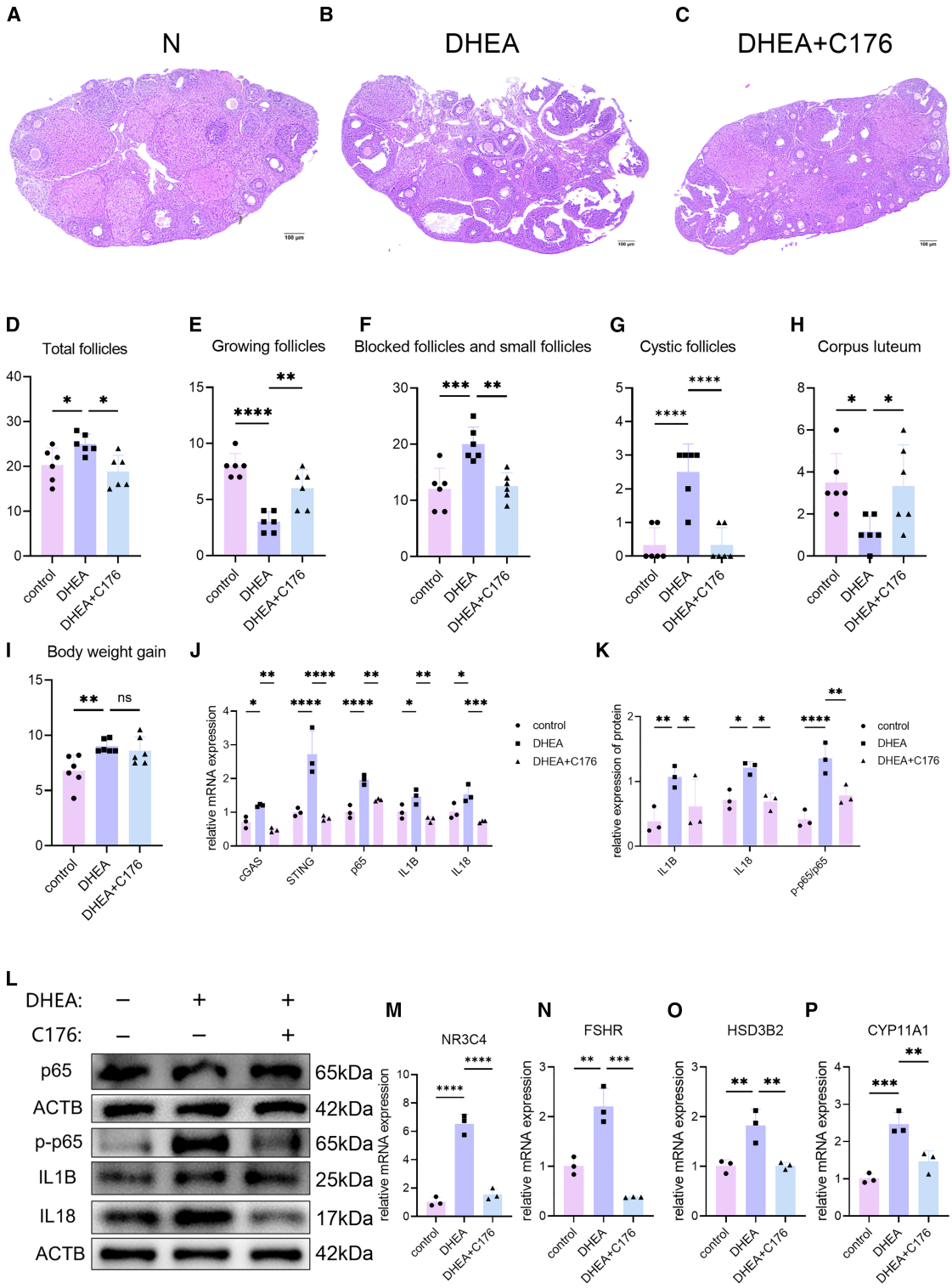

Figure 8. Alleviation of ovarian inflammation and follicle dysfunction after inhibition of STING in DHEA-induced mouse model

(A–C) Representative H&E images of mouse ovary in the mouse injected DHEA and C176 (scale bar, 100 μm, DHEA 60 mg/kg per mouse daily, C176 750 nmol per mouse daily in 200 μL corn oil).

(D–H) Quantification of follicles at all stages and corpus luteum in the mouse injected DHEA and C176 (n = 6).

(I) Quantification of body weight gain in the mouse injected DHEA and C176 (n = 6).

(legend continued on next page)

Perturbations in cellular homeostasis, induced by a myriad of stimuli, can disrupt mitochondrial integrity, leading to mtDNA release into the cytoplasm.[29] Once liberated, mtDNA is recognized by the nucleic acid sensor cGAS, which catalyzes the synthesis of the secondary messenger cGAMP. This molecular event precipitates the activation and translocation of STING, culminating in the phosphorylation and nuclear translocation of transcription factors IRF3 and NFKB. IFNI and IL6 further underscores this inflammatory response.[30]

Within the PCOS context, transmission electron microscopy has revealed the pathological disarray of mitochondria, resulting in the cytosolic accumulation of mtDNA and activation of the cGAS-STING axis. Using both *in vitro* knockdown and *in vitro* inhibition of STING, our investigations have revealed a marked attenuation of T-induced inflammatory indices. These findings substantiate the hypothesis that the mtDNA-cGAS-STING pathway is inextricably linked to the inflammatory milieu characteristic of PCOS.

To exacerbate the inflammation, T plays a significant role in the KGN cells, a model of ovarian GCs. Our findings demonstrate that T can induce inflammation in these cells by activating the mtDNA-cGAS-STING pathway. This highlights the potential for T-mediated inflammation in the pathogenesis of PCOS.

A crucial insight provided herein is the effectiveness of knocking down STING, a key component of the cGAS-STING axis, in reducing T-induced inflammation in KGN cells. This manipulation significantly mitigated the production of pro-inflammatory cytokines, suggesting a promising therapeutic strategy for PCOS-related inflammation.

Furthermore, the study identified mPTP modulation as another method by which the mtDNA-cGAS-STING axis is regulated. By reducing mtDNA release into the cytosol, cGAS-STING axis activation and the subsequent inflammatory response can be inhibited. This finding points toward a balance between mtDNA release and mPTP regulation as a critical factor in managing inflammation.

Finally, this study demonstrates that inhibiting the STING protein can block Dehydroepiandrosterone (DHEA)-induced ovarian inflammation in a mouse model. DHEA is a known trigger of PCOS-like symptoms in rodents; successful of this inhibition in blocking inflammation suggests a translational approach for human PCOS treatment.

The established relation between mPTP opening and mitochondrial homeostasis highlights that during heightened stress, mitochondrial homeostasis is disrupted, triggering mPTP activation. This, in turn, facilitates release of mtDNA into the cytoplasm.[31] This study further reveals that the application of T to KGN cells enhances their mPTP opening. Inhibiting mPTP opening with CsA led to observations of reduced free mtDNA levels, decreased expression of genes and proteins related to the cGAS-STING pathway, and decreased downstream inflammatory markers.

Despite the established physiological significance of mPTP, its precise molecular constituents remain unclear. Nonetheless, recent work by Santhanam et al. revealed that mPTP is a heteromeric protein complex, consisting primarily of SPG7 and CypD. Notably, interrupting the SPG7-CypD interaction significantly mitigates cell death triggered by oxidative stress.[32] Numerous studies have further validated that pharmacological deactivation of mPTP, achieved via CypD inhibition, effectively halts mtDNA escape and accumulation in the cytoplasm.[33]

In conclusion, this study offers significant insights into the activation of ovarian inflammation in PCOS, particularly through the cGAS-STING pathway and the role of mtDNA. The findings suggest new potential targets for treating PCOS-related inflammation, such as inhibiting the STING protein or modulating the mPTP function. These findings also underscore the complexity of PCOS pathogenesis and highlight the promise of molecular interventions to mitigate the inflammation that characterizes this disorder. Future studies could explore these mechanisms further, and assess their clinical applicability in managing PCOS symptoms and improving fertility outcomes for women affected by this condition.

Limitations of the study

There are still many shortcomings in this study. Unfortunately, the number of clinical samples we selected was not sufficient. In the follow-up experiment, we will continue to expand the sample size and try to select transgenic animals for *in vivo* experiment verification. The mechanisms governing how mitochondrial stress modulates the interactions among mPTP components, and the potential role of additional proteins in activating mPTP and subsequently releasing mtDNA into the cytoplasm, remain to be comprehensively elucidated.

RESOURCE AVAILABILITY

The data are available on request from the lead contact upon request.

Lead contact

Further information and requests for resources and reagents should be directed to and will be fulfilled by the lead contact, (hongshange@njmu.edu.cn).

Materials availability

This paper did not produce any unique reagents.

Data and code availability

The data are available on request from the lead contact.

(J) mRNA levels of cGAS, STING, p65, IL1B, and IL18 in the ovarian tissue of mouse injected DHEA and C176 (n = 3).
(K) Quantification of the protein expression levels of p-p65/p65, IL1B, and IL18 in the ovarian tissue of mouse injected DHEA and C176 (n = 3).
(L) Representative western blotting images of p65, p-p65, IL1B, and IL18 in the ovarian tissue of mouse injected DHEA and C176 (n = 3).
(M) mRNA levels of NR3C4 in the ovarian tissue of mouse injected DHEA and C176 (n = 3).
(N) mRNA levels of FSHR in the ovarian tissue of mouse injected DHEA and C176 (n = 3).
(O) mRNA levels of HSD3B2 in the ovarian tissue of mouse injected DHEA and C176 (n = 3).
(P) mRNA levels of CYP11A1 in the ovarian tissue of mouse injected DHEA and C176 (n = 3). Data are represented as mean ± SEM.*p < 0.05, **p < 0.01, ***p < 0.001, ****p < 0.0001.

ACKNOWLEDGMENTS

This work was supported by the National Natural Science Foundation of China (grant number: 81771586) and the Taizhou People's Hospital, Jiangsu Province, China.

AUTHOR CONTRIBUTIONS

J.C. designed and executed the experiment. J.C., Q.Z., and Y.X. analyzed the data and drafted and revised the manuscript. L.W., N.L., X.H., and M.X. assisted with some of the experiments. Corresponding author H.G. participated in the design of the study and reviewed the article.

DECLARATION OF INTERESTS

The authors declare no competing interests.

STAR★METHODS

Detailed methods are provided in the online version of this paper and include the following:

- KEY RESOURCES TABLE
- EXPERIMENTAL MODEL AND STUDY PARTICIPANT DETAILS
  - Ethical approval
  - Collection of clinical samples
- ANIMAL STUDIES
  - Culture and treatment of KGN cells
- METHOD DETAILS
  - Collection and isolation of follicular fluid and ovarian GCs
  - RNA transfection
  - RNA isolation and real-time quantitative polymerase chain reaction
  - Separation and purification of mitochondrial DNA
  - Western blot analysis
  - Immunofluorescence
  - Mitochondrial mPTP open assay
- QUANTIFICATION AND STATISTICAL ANALYSIS

SUPPLEMENTAL INFORMATION

Supplemental information can be found online at https://doi.org/10.1016/j.isci.2025.112391.

Received: August 19, 2024
Revised: November 23, 2024
Accepted: April 4, 2025
Published: April 8, 2025

REFERENCES

1. Dapas, M., and Dunaif, A. (2022). Deconstructing a Syndrome: Genomic Insights Into PCOS Causal Mechanisms and Classification. Endocr. Rev. *43*, 927–965. https://doi.org/10.1210/endrev/bnac001.
2. Patel, S. (2018). Polycystic ovary syndrome (PCOS), an inflammatory, systemic, lifestyle endocrinopathy. J. Steroid Biochem. Mol. Biol. *182*, 27–36. https://doi.org/10.1016/j.jsbmb.2018.04.008.
3. Goodarzi, M.O., Dumesic, D.A., Chazenbalk, G., and Azziz, R. (2011). Polycystic ovary syndrome: etiology, pathogenesis and diagnosis. Nat. Rev. Endocrinol. *7*, 219–231. https://doi.org/10.1038/nrendo.2010.217.
4. Pasquali, R., Stener-Victorin, E., Yildiz, B.O., Duleba, A.J., Hoeger, K., Mason, H., Homburg, R., Hickey, T., Franks, S., Tapanainen, J.S., et al. (2011). PCOS Forum: research in polycystic ovary syndrome today and tomorrow. Clin. Endocrinol. *74*, 424–433. https://doi.org/10.1111/j.1365-2265.2010.03956.x.
5. Herman, R., Jensterle, M., Janež, A., Goričar, K., and Dolžan, V. (2020). Genetic Variability in Antioxidative and Inflammatory Pathways Modifies the Risk for PCOS and Influences Metabolic Profile of the Syndrome. Metabolites *10*, 439. https://doi.org/10.3390/metabo10110439.
6. Li, S., Zhang, L., Wei, N., Tai, Z., Yu, C., and Xu, Z. (2021). Research Progress on the Effect of Epilepsy and Antiseizure Medications on PCOS Through HPO Axis. Front. Endocrinol. *12*, 787854. https://doi.org/10.3389/fendo.2021.787854.
7. Diamanti-Kandarakis, E. (2006). Insulin resistance in PCOS. Endocrine *30*, 13–17. https://doi.org/10.1385/endo:30:1:13.
8. Franks, S., Stark, J., and Hardy, K. (2008). Follicle dynamics and anovulation in polycystic ovary syndrome. Hum. Reprod. Update *14*, 367–378. https://doi.org/10.1093/humupd/dmn015.
9. Faire, M., Skillern, A., Arora, R., Nguyen, D.H., Wang, J., Chamberlain, C., German, M.S., Fung, J.C., and Laird, D.J. (2015). Follicle dynamics and global organization in the intact mouse ovary. Dev. Biol. *403*, 69–79. https://doi.org/10.1016/j.ydbio.2015.04.006.
10. Liu, Y.X., Zhang, Y., Li, Y.Y., Liu, X.M., Wang, X.X., Zhang, C.L., Hao, C.F., and Deng, S.L. (2019). Regulation of follicular development and differentiation by intra-ovarian factors and endocrine hormones. Front. Biosci. *24*, 983–993. https://doi.org/10.2741/4763.
11. Boots, C.E., and Jungheim, E.S. (2015). Inflammation and Human Ovarian Follicular Dynamics. Semin. Reprod. Med. *33*, 270–275. https://doi.org/10.1055/s-0035-1554928.
12. Xiang, Y., Wang, H., Ding, H., Xu, T., Liu, X., Huang, Z., Wu, H., and Ge, H. (2023). Hyperandrogenism drives ovarian inflammation and pyroptosis: A possible pathogenesis of PCOS follicular dysplasia. Int. Immunopharmacol. *125*, 111141. https://doi.org/10.1016/j.intimp.2023.111141.
13. Angajala, A., Lim, S., Phillips, J.B., Kim, J.H., Yates, C., You, Z., and Tan, M. (2018). Diverse Roles of Mitochondria in Immune Responses: Novel Insights Into Immuno-Metabolism. Front. Immunol. *9*, 1605. https://doi.org/10.3389/fimmu.2018.01605.
14. Banoth, B., and Cassel, S.L. (2018). Mitochondria in innate immune signaling. Transl. Res. *202*, 52–68. https://doi.org/10.1016/j.trsl.2018.07.014.
15. Kopinski, P.K., Singh, L.N., Zhang, S., Lott, M.T., and Wallace, D.C. (2021). Mitochondrial DNA variation and cancer. Nat. Rev. Cancer *21*, 431–445. https://doi.org/10.1038/s41568-021-00358-w.
16. Marchi, S., Guilbaud, E., Tait, S.W.G., Yamazaki, T., and Galluzzi, L. (2023). Mitochondrial control of inflammation. Nat. Rev. Immunol. *23*, 159–173. https://doi.org/10.1038/s41577-022-00760-x.
17. Du, M., and Chen, Z.J. (2018). DNA-induced liquid phase condensation of cGAS activates innate immune signaling. Science *361*, 704–709. https://doi.org/10.1126/science.aat1022.
18. Hopfner, K.-P., and Hornung, V. (2020). Molecular mechanisms and cellular functions of cGAS-STING signalling. Nat. Rev. Mol. Cell Biol. *21*, 501–521. https://doi.org/10.1038/s41580-020-0244-x.
19. Ma, X.M., Geng, K., Law, B.Y.-K., Wang, P., Pu, Y.L., Chen, Q., Xu, H.W., Tan, X.Z., Jiang, Z.Z., and Xu, Y. (2023). Lipotoxicity-induced mtDNA release promotes diabetic cardiomyopathy by activating the cGAS-STING pathway in obesity-related diabetes. Cell Biol. Toxicol. *39*, 277–299. https://doi.org/10.1007/s10565-021-09692-z.
20. Liu, Z., Wang, M., Wang, X., Bu, Q., Wang, Q., Su, W., Li, L., Zhou, H., and Liu, L. (2022). XBP1 deficiency promotes hepatocyte pyroptosis by impairing mitophagy to activate mtDNA-cGAS-STING signaling in macrophages during acute liver injury. Redox Biol. *52*, 102305. https://doi.org/10.1016/j.redox.2022.102305.
21. Siemers, K.M., Klein, A.K., and Baack, M.L. (2023). Mitochondrial Dysfunction in PCOS: Insights into Reproductive Organ Pathophysiology. Int. J. Mol. Sci. *24*, 13123. https://doi.org/10.3390/ijms241713123.
22. Dabravolski, S.A., Nikiforov, N.G., Eid, A.H., Nedosugova, L.V., Starodubova, A.V., Popkova, T.V., Bezsonov, E.E., and Orekhov, A.N. (2021). Mitochondrial Dysfunction and Chronic Inflammation in Polycystic Ovary Syndrome. Int. J. Mol. Sci. *22*, 3923. https://doi.org/10.3390/ijms22083923.

23. Ding, H., Xiang, Y., Zhu, Q., Wu, H., Xu, T., Huang, Z., and Ge, H. (2024). Endoplasmic reticulum stress-mediated ferroptosis in granulosa cells contributes to follicular dysfunction of polycystic ovary syndrome driven by hyperandrogenism. Reprod. Biomed. Online *49*, 104078. https://doi.org/10.1016/j.rbmo.2024.104078.

24. Choudhuri, S., Chowdhury, I.H., and Garg, N.J. (2020). Mitochondrial Regulation of Macrophage Response Against Pathogens. Front. Immunol. *11*, 622602. https://doi.org/10.3389/fimmu.2020.622602.

25. Xian, H., Watari, K., Sanchez-Lopez, E., Offenberger, J., Onyuru, J., Sampath, H., Ying, W., Hoffman, H.M., Shadel, G.S., and Karin, M. (2022). Oxidized DNA fragments exit mitochondria via mPTP- and VDAC-dependent channels to activate NLRP3 inflammasome and interferon signaling. Immunity *55*, 1370–1385.e8. https://doi.org/10.1016/j.immuni.2022.06.007.

26. Yu, C.-H., Davidson, S., Harapas, C.R., Hilton, J.B., Mlodzianoski, M.J., Laohamonthonkul, P., Louis, C., Low, R.R.J., Moecking, J., De Nardo, D., et al. (2020). TDP-43 Triggers Mitochondrial DNA Release via mPTP to Activate cGAS/STING in ALS. Cell *183*, 636–649.e18. https://doi.org/10.1016/j.cell.2020.09.020.

27. Liu, Y., Liu, H., Li, Z., Fan, H., Yan, X., Liu, X., Xuan, J., Feng, D., and Wei, X. (2021). The Release of Peripheral Immune Inflammatory Cytokines Promote an Inflammatory Cascade in PCOS Patients via Altering the Follicular Microenvironment. Front. Immunol. *12*, 685724. https://doi.org/10.3389/fimmu.2021.685724.

28. Riley, J.S., and Tait, S.W. (2020). Mitochondrial DNA in inflammation and immunity. EMBO Rep. *21*, e49799. https://doi.org/10.15252/embr.201949799.

29. Kim, J., Kim, H.-S., and Chung, J.H. (2023). Molecular mechanisms of mitochondrial DNA release and activation of the cGAS-STING pathway. Exp. Mol. Med. *55*, 510–519. https://doi.org/10.1038/s12276-023-00965-7.

30. West, A.P., and Shadel, G.S. (2017). Mitochondrial DNA in innate immune responses and inflammatory pathology. Nat. Rev. Immunol. *17*, 363–375. https://doi.org/10.1038/nri.2017.21.

31. Zhang, W., Li, G., Luo, R., Lei, J., Song, Y., Wang, B., Ma, L., Liao, Z., Ke, W., Liu, H., et al. (2022). Cytosolic escape of mitochondrial DNA triggers cGAS-STING-NLRP3 axis-dependent nucleus pulposus cell pyroptosis. Exp. Mol. Med. *54*, 129–142. https://doi.org/10.1038/s12276-022-00729-9.

32. Bonora, M., Giorgi, C., and Pinton, P. (2022). Molecular mechanisms and consequences of mitochondrial permeability transition. Nat. Rev. Mol. Cell Biol. *23*, 266–285. https://doi.org/10.1038/s41580-021-00433-y.

33. Miao, R., Jiang, C., Chang, W.Y., Zhang, H., An, J., Ho, F., Chen, P., Zhang, H., Junqueira, C., Amgalan, D., et al. (2023). Gasdermin D permeabilization of mitochondrial inner and outer membranes accelerates and enhances pyroptosis. Immunity *56*, 2523–2541.e8. https://doi.org/10.1016/j.immuni.2023.10.004.

34. Schneider, C.A., Rasband, W.S., and Eliceiri, K.W. (2012). NIH Image to ImageJ: 25 years of image analysis. Nat. Methods *9*, 671–675. https://doi.org/10.1038/nmeth.2089.

35. West, A.P., Khoury-Hanold, W., Staron, M., Tal, M.C., Pineda, C.M., Lang, S.M., Bestwick, M., Duguay, B.A., Raimundo, N., MacDuff, D.A., et al. (2015). Mitochondrial DNA stress primes the antiviral innate immune response. Nature *520*, 553–557. https://doi.org/10.1038/nature14156.

STAR★METHODS

KEY RESOURCES TABLE

REAGENT or RESOURCE	SOURCE	IDENTIFIER
Antibodies		
Anti-cGAS antibody [EPR26492-84]	Abcam	Cat#ab302617; RRID: AB_3076687
Anti-cGAS antibody [EPR23611-101]	Abcam	Cat#ab252416; RRID: AB_3677536
Anti-NF-kB p65 antibody [E379]	Abcam	Cat#ab32536; RRID: AB_776751
Phospho-NF-κB p65 (Ser536) (93H1) Rabbit mAb	Cell Signaling Technology	Cat#3033s; RRID:AB_331284
STING (D2P2F) Rabbit mAb	Cell Signaling Technology	Cat#13647; RRID: AB_2732796
IL-1 Beta Polyclonal antibody	Proteintech	Cat#16806-1-AP; RRID: AB_10646432
IL-18 Polyclonal antibody	Proteintech	Cat#10663-1-AP; RRID: AB_2123636
TMEM173/STING Polyclonal antibody	Proteintech	Cat#19851-1-AP; RRID: AB_10665370
Beta Actin Monoclonal antibody	Proteintech	Cat#66009-1-Ig; RRID: AB_2687938
HRP-conjugated Goat Anti-Mouse IgG(H + L)	Proteintech	Cat#SA00001-1; RRID: AB_2722565
HRP-conjugated Goat Anti-Rabbit IgG(H + L)	Proteintech	Cat#SA00001-2; RRID: AB_2722564
Alexa Fluor® 594 AffiniPure® Fab Fragment Goat Anti-Rabbit IgG (H + L)	Jackson ImmunoResearch Labs	Cat#111-587-003; RRID: AB_2338071
Biological samples		
Human follicular fluid	This paper	N/A
Human granulosa cells	This paper	N/A
Chemicals, peptides, and recombinant proteins		
Dulbecco's Modified Eagle's Medium/F12 medium	KeyGENBioTECH	Cat# KGL1201-500
Fetal bovine serum	Sigma	Cat#F0193
Testosterone	APExBIO Technology LLC	Cat#C6163
Cyclosporin A	MedChemexpress	Cat#HY-B0579
TRIzol	TIANGEN	Cat# DP424
SuperReal PreMix Plus	Vazyme	Cat#Q311
Reverse-transcribed kit	Applied Biological Materials	Cat#G490
4% paraformaldehyde	Solarbio	Cat#P1110
QuickBlock™Immunostaining blocking solution	Beyotime	Cat#P0260
DAPI	Servicebio	Cat#G1012
Critical commercial assays		
Mitochondrial DNA extraction kit	Abcam	Cat#ab65320
Tissue and Blood DNA Extraction kit	QIAGEN	Cat#69504
Mitochondrial permeability transition pore test kit	Beyotime	Cat#C2009
Deposited data		
RNA-seq data	This paper	N/A
Experimental models: Cell lines		
Human ovarian GC line (KGN)	Zhong-qiao Xinzhou Biotechnology CO.LTD	ZQ0916
Experimental models: Organisms/strains		
ICR mouse	HANJIANG BIOTECHNOLOGY CO.LTD	N/A
Oligonucleotides		
siRNA targeting sequence see Table S1	This paper	N/A
Primers used in RT-qPCR see Table S2	This paper	N/A
Software and algorithms		
GraphPad Prism 9	GraphPad Prism Software, Inc	https://www.graphpad.com/
ImageJ software	Schneider et al.[34]	https://imagej.net/software/fiji/

EXPERIMENTAL MODEL AND STUDY PARTICIPANT DETAILS

Ethical approval

The clinical study was approved by the Institutional Review Committee of the Taizhou People's Hospital (KY2022-162-01). Animal research has been approved by the Experimental Animal Ethics Committee of Jiangsu Hanjiang Biotechnology Co., LTD. (HJSW-2024021101).

Collection of clinical samples

The healthy control group (n = 23) and patients with PCOS with hyperandrogenemia (n = 23), all aged 20–35 years, all of whom were undergoing *in vitro* fertilization (IVF)/intracytoplasmic sperm injection (ICSI) treatment, were recruited from our hospital's reproductive center and informed consent was obtained from all participants before they began the study. The patient group qualified for the 2003 Rotterdam criteria and met one of the following characteristics: oligo ovulatory or anovulation, based on ultrasound examination of polycystic changes in the ovaries.

The healthy control group included women with tubal infertility or who were undergoing IVF. These women had normal ovarian function and endocrine indexes. Potential control participants who had an infectious disease or were taking antibiotics before or during IVF treatment were excluded.

Follicle-stimulating hormone (FSH), luteinizing hormone (LH), anti-Müllerian hormone (AMH), total testosterone (T), estrogen, and progesterone levels were measured for all participants on menstrual cycle days 2–4. Data collected included age, body mass index, total cholesterol, fasting blood glucose, and white blood cell count (Table 1). Three samples were randomly selected from each group for RNA-seq analysis. The specific process is shown in Figure 1.

ANIMAL STUDIES

Eighteen three-week-old female mice were carefully chosen and subsequently allocated at random into three groups: a control group, a PCOS model group, and an STING-inhibited model group. To induce PCOS-like characteristics, each PCOS group mouse received subcutaneous injections of dehydroepiandrosterone (DHEA) at a dose of 60 mg/kg/day over a period of 28 days.[12] To inhibit STING, each mouse received intraperitoneal injection of C176 at a dose of 750 nmol per mouse daily in 200 μL corn oil over a period of 28 days. The animals were monitored for symptoms resembling those of PCOS, including ovarian cyst formation. Upon conclusion of the study, the mice were humanely sacrificed, and relevant tissues, including ovaries, were harvested for further examination and analysis.

Culture and treatment of KGN cells

KGN cells were cultivated in DMEM/F12, supplemented with 10% FBS and 1% penicillin/streptomycin at 37°C, in an incubator containing 5% carbon dioxide. To assess the impact of hyperandrogen secretion by KGN cells on inflammation, the cells were exposed to 10 μM T (APExBIO, USA) for 24 h.[12] To further investigate the link between hyperandrogenemia, inflammation, and mPTP opening levels, the mPTP inhibitor CsA (MCE, 10 μM) was introduced into the treatment regimen.

METHOD DETAILS

Collection and isolation of follicular fluid and ovarian GCs

Follicular fluid (FF) and ovarian GCs were collected from subjects using a standardized GnRH antagonist regimen for ovulation induction. When dominant follicles measuring 18 mm or larger were detected, participants received an intramuscular injection of 6000 IU of human chorionic gonadotropin to induce ovulation. Thirty-six hours later, an ovulation extractor was used to collect the first tube of blood-free FF for subsequent enzyme-linked immunosorbent assay testing. The remaining FF was processed to isolate and extract ovarian GCs using a density gradient method. These cells were stored at −80°C for subsequent protein and mRNA extraction.

RNA transfection

To suppress STING, KGN cells were transfected with 30 nM siSTING using transfection reagents for 24 h, then immediately exposed to 10 μM T. The sequences are listed in Table S2.

RNA isolation and real-time quantitative polymerase chain reaction

Cellular RNA was extracted using TRIzol reagent (Tiangen, China) and reverse-transcribed into cDNA by a reverse-transcribed kit (Applied Biological Materials, Canada). Real-time quantitative polymerase chain reaction (qPCR) was performed on a Roche LightCycler (Roche, Basel, Switzerland) using SuperReal PreMix Plus (SYBR Green) (Vazyme, Nanjing, China). The threshold cycle value[4] was used to determine the gene expression level. Then, using beta actin (ACTB) as the reference parameter, the formula $2^{\Delta\Delta}$Ct was calculated. The sequences of all primers used herein are in Table S2.

Separation and purification of mitochondrial DNA

Based on previous research,[35] the cells were first divided into two equal portions. Whole cell genomic DNA was extracted from one group using a centrifuge column and a commercial DNA extraction kit. For the other group, a specific mitochondrial DNA (mtDNA) extraction kit (Abcam, Cambridge, UK) was used to separately extract and purify the mtDNA. To obtain pure cytoplasmic components, the cytoplasm was separated from the nucleus, mitochondria, and ER by high-speed centrifugation. Subsequently, DNA was isolated from these cytoplasmic fractions using the Qiagen Tissue and Blood DNA Extraction kit (Germany). qPCR was then conducted on both the whole cell extracts and the purified cytoplasmic components. qPCR used primers specific to the human B2M gene and mtDNA (Dloop and ND1).

Western blot analysis

Total protein was extracted from GCs, KGN cells and mouse ovary. Electrophoresis was performed on a gel, and the proteins were transferred onto PVDF membranes. After blocking with 5% skim milk for 2 h at room temperature, the membrane was incubated with primary antibody overnight at 4°C. The membrane was then incubated with the secondary antibody HRP Goat Anti-Rabbit IgG (SA00001-2, Proteintech) or HRP-conjugated Affinipure Goat Anti-Rat IgG (SA00001-1, Proteintech) for 2 h at room temperature. After washes, the blots were visualized using chemiluminescence detection (Tanon, Shanghai, China). ImageJ software was used to quantify WB band intensities.

Immunofluorescence

Cells were fixed with 4% paraformaldehyde to preserve their structures and prevent protein degradation. To allow antibodies to access their target molecules within the cell, the sample underwent permeabilization using 2% Triton, which disrupts the cell membrane without damaging the underlying structures. After blocking for 1 h, primary antibodies specific to the target molecules were added to the sample and allowed to bind overnight at 4°C. Unbound primary antibodies were removed by washing the sample several times with PBS. Alexa Fluor-conjugated secondary antibodies were added to the sample and incubated for 1–2 h at room temperature. Unbound secondary antibodies were removed by washing the sample several times with PBS. Samples were then mounted on microscope slides using a mounting medium like DAPI-containing mounting solution. Stained samples were examined using a fluorescence microscope equipped with appropriate filters for detecting the fluorophores used in the labeling process. Images were captured using digital cameras.

Mitochondrial mPTP open assay

The Beyotime mPTP test kit (China) was used to detect mitochondrial mPTP. Treated cells were initially washed with PBS and subsequently incubated with calcein AM and Co^{2+} quencher at 37°C for 30 min. The cells were then cultured in a dye-free medium at 37°C in the dark for an additional 30 min. The resulting observations were made under a fluorescence microscope.

QUANTIFICATION AND STATISTICAL ANALYSIS

The data are presented as mean ± standard error of the mean. Analyses were conducted using GraphPad Prism (GraphPad Inc, USA). One-way and two-way analysis of variance (ANOVA) were used, as appropriate, to test for statistically significant between-groups differences. Tukey's post hoc test was used to compare all possible pairs and determine which differences were statistically significant. $p < 0.05$ was considered statistically significant.